Available online at www.sciencedirect.com
ScienceDirect
Scripta Materialia 61 (2009) 423–426
Scripta MATERIALIA
www.elsevier.com/locate/scriptamat

Al-rich bulk metallic glasses with plasticity and ultrahigh specific strength

B.J. Yang,[a] J.H. Yao,[a] J. Zhang,[a] H.W. Yang,[a] J.Q. Wang[a,*] and E. Ma[b,*]

[a] *Shenyang National Laboratory for Materials Science, Institute of Metal Research, Chinese Academy of Sciences, 72 Wenhua Road, Shenyang 110016, China*

[b] *Department of Materials Science and Engineering, Johns Hopkins University, Baltimore, MD 21218, USA*

Received 12 April 2009; revised 21 April 2009; accepted 21 April 2009
Available online 3 May 2009

Aluminum-based amorphous metals are interesting lightweight alloys with superior mechanical and corrosion properties, but have never been achieved in bulk form. Here we report the first success of obtaining Al-rich (86 at.% Al) bulk metallic glasses (BMGs), based on an alloy composition designed from the preferable internal glass structure. The Al BMGs discovered exhibit ultrahigh specific strength, as well as obvious plasticity.

Keywords: Aluminum alloys; Metallic glasses; Specific strength; Plastic deformation

Ever since the discovery of melt-spun Al-based metallic glass ribbons in 1988 [1,2], there has been a continuous and relentless pursuit of Al-rich bulk metallic glasses (BMGs). The numerous attempts have been unsuccessful so far [3–10], while in a variety of other alloy systems dramatic progress has been made in developing BMGs since the early 1990s [11–14]. It has been realized that Al-based metallic glasses are very different from most of the known bulk glass formers. For example, the glass-forming compositions in Al-based systems are clearly located well away from their eutectic points, from which the liquidus temperature rises steeply. Consequently, the Al glasses exhibit a low reduced glass transition temperature ($T_{rg} < 0.5$, where $T_{rg} = T_g/T_l$, and T_g and T_l are the glass transition temperature and the liquidus temperature, respectively) [13,15].

Our design of potential BMG-forming Al alloy compositions has been guided by recent progress in understanding the internal structure of metallic glasses [16–18]. In particular, our experimental and modeling studies of multicomponent Al-based metallic glasses have revealed the important role of solute-centered quasi-equivalent clusters, the solute species being typically rare earth (RE) and transition metal (TM) elements [19]. One can use cluster combinations to derive an estimate of a composition that is structurally favorable for glass stability and glass-forming ability (GFA). The first step is to predict a favorable ternary composition, and this work started with the case of Al–Ni–Y. It is known from Ref. [19] that for the Al–Ni and Al–La binaries, $Al_{9.4}Ni$ (in atomic ratio) and $Al_{16.9}Y$ clusters are preferred, respectively. The question is then which composition is favorable in the ternary system, without upsetting these preferable ratios. In the ternary alloy phase diagram (composition triangle) shown in Figure 1, we introduce Ni into Al–Y by increasing the Ni content along the composition line linking the Ni apex and the $Al_{16.9}Y$ composition, such that the desired $Al_{16.9}Y$ ratio is maintained. Meanwhile, consider the Y addition into the Al–Ni binary. In this case, we move along the composition line linking the Y apex and the $Al_{9.4}Ni$ composition, so as to retain the $Al_{9.4}Ni$ ratio. At the intersection of these two lines (Fig. 1), i.e. at the composition $Al_{85.8}Ni_{9.1}Y_{5.1}$, both of the desirable atomic composition ratios (Al:Y = 16.9 and Al:Ni = 9.4) are satisfied, as the same (and all of the) Al solvent atoms are shared by both the Ni and Y solutes. The structure is then thought to be composed of interpenetrating, energetically favored solute-centered clusters. This structurally favorable composition, $Al_{85.8}Ni_{9.1}Y_{5.1}$ (see inset in Fig. 1), is then a likely candidate for easy glass formation in the Al–Ni–Y system.

In our experiments, elemental pieces with purity better than 99.9% (99% for Y and La) were used as starting

* Corresponding authors. Tel./fax: +86 24 23971902; e-mail addresses: jqwang@imr.ac.cn; ema@jhu.edu

1359-6462/$ - see front matter © 2009 Acta Materialia Inc. Published by Elsevier Ltd. All rights reserved.
doi:10.1016/j.scriptamat.2009.04.035

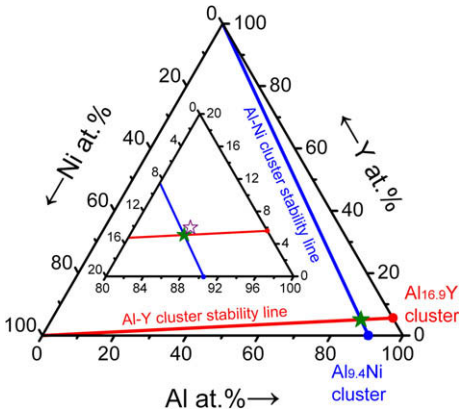

Figure 1. An illustration of our composition design scheme using the cluster stability lines in the Al–Ni–Y ternary alloy phase diagram. The two lines corresponding to the ternary addition to the two respective binary clusters are shown for the whole system and the Al-rich corner (inset). The green star symbol at the intersection of the two lines is the favorable composition predicted, and the purple open star is the experimentally determined optimum glass former.

materials. The master alloy ingots with the nominal composition (in at.%) were prepared by arc melting under a Ti-gettered argon atmosphere in a water-cooled copper crucible. The alloy ingots were melted six times to ensure compositional homogeneity. For rapidly solidified ribbons, samples were prepared with a cross-section of 0.03–0.26 × 3 mm^2 using a single roller melt-spinning technique in an argon atmosphere. Wedge-shaped samples were prepared by casting molten alloys into a wedge-shaped mold with an included angle of 5°. Rod-shaped samples were cast by the injection of the molten alloy into the cavity of a copper mold with a diameter of 1 mm and length of 30 mm. The axial cross-section surfaces of the as-cast rods were investigated by X-ray diffraction (XRD) using a Rigaku D/max 2400 diffractometer (Tokyo, Japan) with monochromated Cu K_α radiation ($\lambda = 0.1542$ nm). The glass transition and crystallization of the alloys were analyzed using differential scanning calorimetry (DSC) in a Perkin-Elmer DSC7 calorimeter under flowing purified argon at a heating rate of 20 K min^{-1}. The melting behavior of the alloys was studied using a Netzsch DSC 404C at a heating rate of 20 K min^{-1}. Samples for conventional and high-resolution transmission electron microscopy (TEM) observations in a FEI Tecnai F30 electron microscope were thinned electrolytically by jet polishing in a mixed 1/4 nitric and 3/4 methanol solution at 243 K. The compression test samples 2 mm in height were cut from the 1 mm diameter injection-cast rods. The loading surfaces were polished to be parallel to an accuracy of less than 10 μm. Uniaxial compressive tests at room temperature were performed on a Shimadzu AG-I machine with an initial strain rate of 1×10^{-4} s^{-1}. At least five samples have been measured to ensure that the results are reproducible. The strain was determined from the platen displacement after correction for machine compliance. The axial cross-section of the as-cast rods and the fracture surfaces of the specimens after compression were examined by scanning electron microscopy (SEM) and energy dispersive X-ray (EDX) analysis using a LEO Supra 35 microscope. The density of the bulk alloys was measured using the Archimedes method.

Through a systematic survey of alloys near the predicted composition $Al_{85.8}Ni_{9.1}Y_{5.1}$, the best glass former in the ternary system is experimentally determined to be $Al_{86}Ni_8Y_6$. As seen in inset of Figure 1, this is very close to the predicted composition. For melt spinning, the critical thickness of the fully amorphous ribbon at this composition is 260 μm. An amorphous structure with critical thickness of about 600 μm can be obtained under wedge casting conditions for this alloy, similar to another Al-based ternary glass [9]. The XRD spectra showing the amorphous features of these alloys are displayed in Figure 2a.

We further improve the GFA by introducing additional solutes in partial substitution for Ni and Y. It is well known that multicomponent additions are effective in elevating the GFA [5,20]. Here we conduct such solute substitution (TM to substitute for Ni, RE for Y) without deviating greatly from the predicted composition ($Al_{85.8}TM_{9.1}RE_{5.1}$). For TM solutes, we know that Al–Co and Al–Ni clusters have similar atomic packing

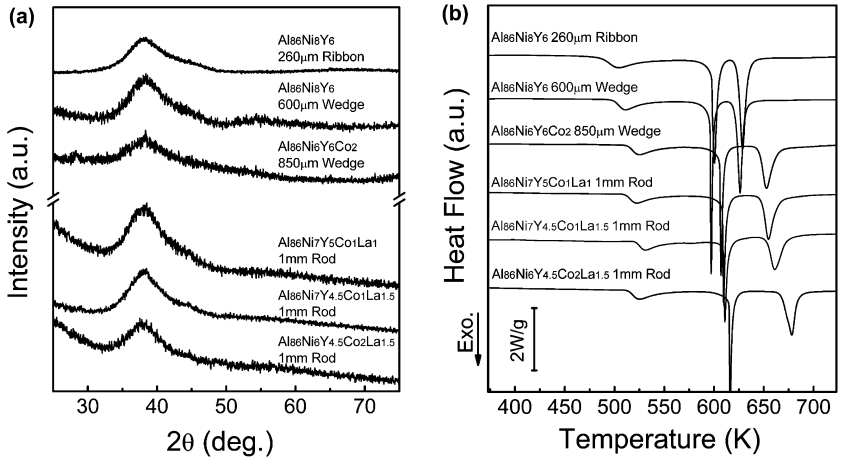

Figure 2. (a) XRD patterns and (b) DSC traces taken from a series of the Al-based glassy alloys from the ternary to the quinary system, for as-spun ribbons, wedge-casting samples and as-cast rods 1 mm in diameter. The DSC heating rate is 20 K min^{-1}.

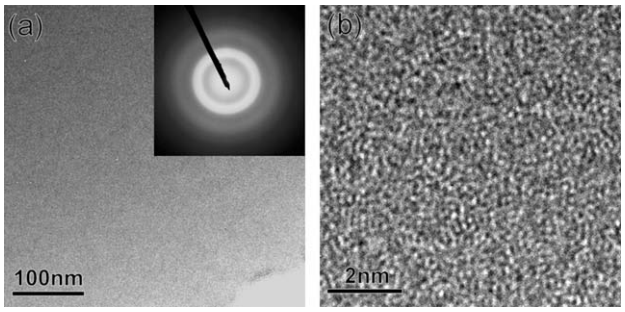

Figure 3. (a) TEM and (b) high-resolution TEM images for the $Al_{86}Ni_7Y_{4.5}Co_1La_{1.5}$ BMGs. The inset shows the corresponding SAED pattern. The sample was taken from the center of the 1 mm as-cast rod.

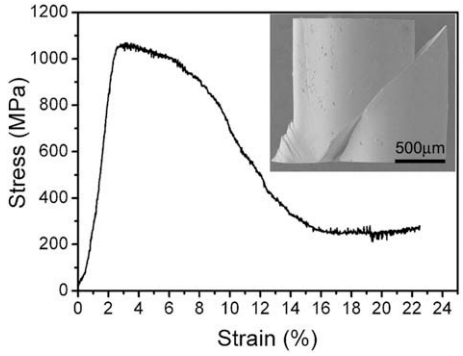

Figure 4. Compressive engineering stress–strain curves of the 1 mm as-cast rod of the $Al_{86}Ni_7Y_{4.5}Co_1La_{1.5}$ BMG. The inset is the SEM image showing the side view of the sample after the test.

configurations, and the number of nearest Al neighbors (coordination number) of Ni and Co are both 9.4 in the two types of clusters [19]. Therefore, Co is added to partially substitute for Ni in the base $Al_{86}Ni_8Y_6$ alloy, with the composition ratio of Al:(NiCo):Y fixed. An $Al_{86}Ni_6Co_2Y_6$ alloy was found to have a glass-forming critical thickness of 850 μm for wedge casting; the XRD spectra of this glass is shown in Figure 2a (The occasional presence of a small amount of the primary α-Al phase in the spectra for the wedge-cast samples is because the fully amorphous region is too thin to be scanned in XRD). We next substituted some of the Y with La (La has a similar coordination number of 17.5 [19]). Fully glassy rods with 1 mm diameter have been successfully obtained at $Al_{86}Ni_6Y_{4.5}Co_2La_{1.5}$. By simultaneously tuning the substituting solutes, 1 mm as-cast BMG rods have also been obtained at $Al_{86}Ni_7Y_5Co_1La_1$ and $Al_{86}Ni_7Y_{4.5}Co_1La_{1.5}$. The XRD patterns of these BMGs have also been included in Figure 2a.

DSC scans were used to further study these samples. Figure 2b displays representative DSC curves for the whole series of alloys shown in Figure 2a from the ternary to the quinary system. The exothermic crystallization signals are clearly seen. It is noted that the crystalline behaviors are similar for these alloys. There are no obvious glass transition endotherms in these DSC traces.

The high-resolution TEM image and the inset selected-area electron diffraction (SAED) pattern for alloy $Al_{86}Ni_7Y_{4.5}Co_1La_{1.5}$ are presented in Figure 3. The sample was taken from the center of the 1 mm as-cast rod. No crystals are visible in the high-resolution TEM image, and the glass appears to be rather uniform on nanometer scale. The broad halo in the SAED pattern indicates the presence of a single amorphous phase, which agrees well with the XRD result that the sample is fully amorphous.

Figure 4 presents the room-temperature compressive engineering stress–strain curves for the 1 mm diameter glassy alloy $Al_{86}Ni_7Y_{4.5}Co_1La_{1.5}$, and the inset shows the SEM image of the sample after the compression test. The $Al_{86}Ni_7Y_{4.5}Co_1La_{1.5}$ glass exhibits a very high yield strength of 1050 MPa. This corresponds to a specific strength of 3.34×10^5 Nm kg^{-1} (this BMG has a mass density of 3.14 g cm^{-3}), higher than that of existing engineering alloys [21]. The strain is concentrated along a localized main shear band, which shows a shear angle of about 45° to the compressive axis. The decrease in the nominal stress after the initial yielding should be attributed to the decrease in the contact (effective loading) area in the shear plane as the shear slip proceeds between the top half of the sample and the bottom half. The subsequent large load drop is likely due to damage formation (such as cracking due to the bending moment as the sample is no longer under uniaxial loading after the relatively large shear offset). The load (the apparent nominal stress) does not continue to drop to zero, and can in fact increase when the sheared top part eventually touches the loading platen, resulting in an increase in the contact area and consequently requiring increased load for deformation [22]. Such spurious effects in the stress–strain curves have been demonstrated recently by Mondal et al. [23] for "ductile" Zr-based BMGs. From the sequence of events observed in Figure 4, especially the shape of the curve for the first several per cent of the plastic deformation, we believe that there is a stage of stable shear band deformation for about 4% of plastic strain, with gradual advancement of the shear. This illustrates that this Al-based BMG can sustain obvious plastic deformation, in a manner similar to some "ductile" BMGs [22,23], and is unlike some brittle BMGs which undergo catastrophic failure immediately after the onset of shear banding.

This research was supported by the National Natural Science Foundation of China (Nos. 50471076 and 50323009) and the National Key Basic Research Program of China (Grant No. 2007CB613906). The authors were part of the MANS Research team, supported in part by the Chinese Academy of Sciences.

[1] Y. He, S.J. Poon, G.J. Shiflet, Science 241 (1988) 1640.
[2] A.P. Tsai, A. Inoue, T. Masumoto, Metall. Trans. A 19 (1988) 1369.
[3] A. Inoue, N. Matsumoto, T. Masumoto, Mater. Trans. JIM 31 (1990) 493.
[4] Y. He, G.M. Dougherty, G.J. Shiflet, S.J. Poon, Acta Metall. Mater. 41 (1993) 337.
[5] A. Inoue, Prog. Mater Sci. 43 (1998) 365.
[6] Z.C. Zhong, A.L. Greer, Int. J. Non-Equilib. Process. 11 (1998) 35.

[7] A.K. Gangopadhyay, K.F. Kelton, Philos. Mag. A 80 (2000) 1193.
[8] F.Q. Guo, S.J. Poon, G.J. Shiflet, Mater. Sci. Forum 331-337 (2000) 31.
[9] W.S. Sanders, J.S. Warner, D.B. Miracle, Intermetallics 14 (2006) 348.
[10] H. Yang, J.Q. Wang, Y. Li, Philos. Mag. 87 (2007) 4211.
[11] A. Inoue, K. Kita, T. Zhang, T. Masumoto, Mater. Trans. JIM 30 (1989) 722.
[12] A. Peker, W.L. Johnson, Appl. Phys. Lett. 63 (1993) 2342.
[13] A. Inoue, Acta Mater. 48 (2000) 279.
[14] A.L. Greer, E. Ma, MRS Bull. 32 (2007) 611.
[15] D. Turnbull, Contemp. Phys. 10 (1969) 473.
[16] D.B. Miracle, Nat. Mater. 3 (2004) 697.
[17] A.P. Wang, J.Q. Wang, E. Ma, Appl. Phys. Lett. 90 (2007) 121912.
[18] C. Dong, J.B. Qiang, Y.M. Wang, N. Jiang, J. Wu, P. Thiel, Philos. Mag. 86 (2006) 263.
[19] H.W. Sheng, Y.Q. Cheng, P.L. Lee, S.D. Shastri, E. Ma, Acta Mater. 56 (2008) 6264.
[20] A.L. Greer, Science 267 (1995) 1947.
[21] M.F. Ashby, in: Materials and Process Selection Charts, Appendix to Materials Selection in Mechanical Design, Pergamon Press, Oxford, 1993, p. 8.
[22] S.X. Song, H. Bei, J. Wadsworth, T.G. Nieh, Intermetallics 16 (2008) 813.
[23] K. Mondal, G. Kumar, T. Ohkubo, K. Oishi, T. Mukai, K. Hono, Philos. Mag. Lett. 87 (2007) 625.